Original Article

Total gadolinium tissue deposition and skin structural findings following the administration of structurally different gadolinium chelates in healthy and ovariectomized female rats

Yì-Xiáng J. Wáng[1], Joseph Schroeder[2], Heiko Siegmund[2], Jean-Marc Idée[3], Nathalie Fretellier[3], Gaëlle Jestin-Mayer[3], Cecile Factor[3], Min Deng[1], Wei Kang[4], Sameh K. Morcos[5]

[1]Department of Imaging and Interventional Radiology, Faculty of Medicine, The Chinese University of Hong Kong, Prince of Wales Hospital, New Territories, Hong Kong SAR, China; [2]Central EM Laboratory, Institute of Pathology, Uniklinikum Regensburg, The University of Regensburg, Germany; [3]Guerbet, Research and Innovation Division, BP 57400, 95943 Roissy-Charles de Gaulle cedex, France; [4]Department of Anatomical and Cellular Pathology, Faculty of Medicine, The Chinese University of Hong Kong, Prince of Wales Hospital, New Territories, Hong Kong SAR, China; [5]Department of Diagnostic Imaging, The University of Sheffield, Sheffield, UK

Correspondence to: Dr Yì-Xiáng J. Wáng. Department of Imaging and Interventional Radiology, Faculty of Medicine, The Chinese University of Hong Kong, Prince of Wales Hospital, New Territories, Hong Kong SAR, China. Email: yixiang_wang@cuhk.edu.hk.

Objective: To assess the retention of gadolinium (Gd) in skin, liver, and bone following gadodiamide or gadoteric acid administration.

Methods: Gd was measured in skin, liver and femur bone in female rats 10 weeks after administration of 17.5 mmol Gd/kg over 5 days of Gd agents. Rat skin microscopy, energy filtering transmission electron microscopy and elemental analysis were performed, and repeated after receiving the same dosage of gadodiamide in rats with osteoporosis induced with bilateral ovariectomy (OVX). The OVX was performed 60 days after the last injection of gadodiamide and animals sacrificed 3 weeks later.

Results: Gd concentration was 180-fold higher in the skin, 25-fold higher in the femur, and 30-fold higher in the liver in rats received gadodiamide than rats received gadoteric acid. The retention of Gd in the skin with gadodiamide was associated with an increase in dermal cellularity, and Gd encrustation of collagen fibers and deposition inside the fibroblasts and other cells. No differences in Gd concentration in liver, skin, and femur were observed between rats receiving gadodiamide with or without OVX.

Conclusions: Gd tissue retention with gadodiamide was higher than gadoteric acid. Tissues Gd deposition did not alter following gadodiamide administration to ovariectomized rats.

Keywords: Gadolinium (Gd); skin; ultrastructural; bone deposition; osteoporosis

Submitted May 15, 2015. Accepted for publication May 22, 2015.
doi: 10.3978/j.issn.2223-4292.2015.05.03
View this article at: http://dx.doi.org/10.3978/j.issn.2223-4292.2015.05.03

Introduction

It is generally accepted that a strong binding of the ligand to the lanthanide gadolinium (Gd^{3+}) is important for the safety of gadolinium based contrast agents (GBCA), widely used in magnetic resonance imaging (MRI) since Gd^{3+} is highly acutely toxic (1-4). The binding of the polyaza-polycarboxylic ligand to Gd^{3+} is relatively weak in the non-ionic linear chelates whereas the macrocyclic chelates offer better binding with lower propensity to release free toxic Gd^{3+} ions over the time (1-7). Retention of gadolinium in Gd^{3+} in body tissues has been used to assess the stability of GBCAs *in vivo* (8-15). Gd^{3+} detected in tissues 5 days after

administration of a GBCA is likely to be gradually released from the chelate and the lower the stability of the GBCA, the higher the retention of gadolinium in tissues. Tweedle *et al.* found that Gd^{3+} retention in liver and bone 2 weeks after injection of GBCAs was three times greater following the linear and non-ionic GBCA gadodiamide (Omniscan®) compared to the linear and ionic GBCA gadopentetic acid (Magnevist®). In both mice and rats, total Gd^{3+} retention in tissues was minimal with the macrocyclic chelates gadoteric acid (Dotarem®) and gadoteridol (ProHance®) (8). Wadas *et al.* showed difference deposition of Gd^{3+} in different tissues in control or renal-impaired transgenic mice after administration of GBCAs of different stability. In animals with renal impairment, the retention of Gd^{3+} in tissues was markedly higher than in animals with normal renal function, while the macrocyclic GBCA caused significantly lower accumulation of Gd^{3+} than the non-ionic linear agent in renally-impaired mice (10).

The long-term retention of Gd^{3+} in the skin after repeated GBCA administrations has been investigated in healthy (11) and renally-impaired (12-16) rats. In healthy rats, the retention of Gd^{3+} in the skin could be found throughout the 12 months observation period with linear GBCAs but not macrocyclic chelates (11). The extent of retention correlated with the GBCA thermodynamic stability and followed the order gadodiamide > gadoversetamide (OptiMARK®) > gadopentetic acid, while only minimal amount of Gd^{3+} retention was observed with macrocyclic GBCAs gadobutrol (Gadovist®), gadoteridol (ProHance®) and gadoteric acid (11). The persistence of Gd^{3+} in skin tissue for such a long time may suggest that it is, at least in part, in insoluble form. However, there is evidence that linear GBCAs gradually release Gd^{3+} which is present in tissues in the soluble form (12,15). In fact, these two possibilities are not mutually exclusive (17).

In human, Gd^{3+} retention in tissues has been demonstrated in patients with nephrogenic systemic fibrosis, a serious iatrogenic disease observed in patients with severe or end-stage kidney disease who received GBCA (almost exclusively linear chelates) for MRI (17-23). Gd^{3+} retention in bone tissues has also been reported in patients with normal renal function who had received a GBCA (24,25). In one study, Gd^{3+} was demonstrated to be retained in bone tissue for longer than 8 years (25). The bone accumulation was about four times greater after a non-ionic linear Gd^{3+} chelate than after a non-ionic macrocyclic Gd^{3+} chelate in patients with normal renal function (24). The long-term implications of Gd^{3+} deposition in bone tissue have yet to be determined. It is possible that Gd^{3+} might impact negatively bone homeostasis similar to that associated with other toxic metals such as lead or cadmium (26). The release of Gd^{3+} into the blood circulation is another possibility, as a consequence of bone resorption such as in patients developing osteoporosis (25). Released Gd^{3+} ions might bind plasma proteins and/or endogenous anions. Insoluble Gd^{3+} would eventually be trapped by the reticuloendothelial system (RES) in splenic macrophages, liver Kupffer cells and hepatocytes, as reported after administration of a soluble Gd^{3+} salt to rats (27). Extensive non-clinical studies concerning the safety and long term effects of repeated injections of GBCAs have been reported (28) but, to our knowledge, the models selected never included osteoporotic animals.

In the present study, we investigated the extent of Gd^{3+} deposition in liver, skin and bone in adult female rats following multiple injections of high cumulated dosage of a low- or high-thermodynamic stability GBCA, focusing on the structural changes in the skin that develop in association with Gd^{3+} retention. The possibility that osteoporosis may impact Gd^{3+} retention in tissues of gadodiamide-treated rats was also investigated.

Materials and methods

Animals

The protocols and procedures were approved by the local Animal Experimentation Ethics Committee. A total of 48 female Sprague-Dawley (SD) rats weighting 220-245 g were used. Two to three animals were housed per stainless steel cage on a 12-h light/12-h dark cycle in an air-conditioned room at 22 ℃, and check daily by the animal care staff. A standard rat chow and water were available ad libitum.

Phase 1 study

This phase was to determine the extent of Gd^{3+} deposition in bone, skin and liver after exposure to the non-ionic linear GBCA gadodiamide (Omniscan®, GE Healthcare, Amersham, UK) or the ionic macrocyclic agent gadoteric acid (Dotarem®, Guerbet, Roissy, France) in rats. Twenty-four rats were used and were randomly divided into three groups (8/group). A cumulated dose of 17.5 mmol Gd/kg was given over 5 days (n=8/group) with tail vein injection of gadodiamide or gadoteric acid, while control rats received normal saline (n=8). Skin biopsy from the dorsal surface

was performed prior to GBCA injection. During these procedures, brief anaesthesia was induced by 3% isoflurane. Animals were sacrificed 10 weeks after the last injection as plateau of Gd^{3+} concentration in the skin is reached 60 days after GBCA injection (11), and skin from the dorsal surface, liver and both femurs were collected.

Phase 2 study

The aim of this study was to determine Gd^{3+} deposition in tissues after exposure to gadodiamide in rats before and after the development of osteoporosis. Only gadodiamide was used as, in phase one study, virtually no Gd^{3+} bone retention was observed in gadoteric acid treated rats. Injection of gadodiamide followed the same dosage regime as in phase one. Sixty days later, gadodiamide-treated rats were divided into two sub-groups with (n=8) or without (n=8) ovariectomy (OVX). Skin biopsy from the dorsal surface of the rat was performed before gadodiamide injection, and at the time of OVX which was performed 60 days after gadodiamide injection (i.e., Day 80). Control rats (n=8) received saline and OVX.

For surgery, the rats were anaesthetized using a combination of xylazine (10 mg/kg) and ketamine (90 mg/kg). Bilateral OVX was performed using an incision 1.5 cm inferior to the costal margin. Ovaries together with surrounding fat tissue were removed. The incision was closed using muscle and skin sutures. Success of OVX was confirmed at necropsy by noting an absence of ovarian tissue and atrophy of uterine horns (29-31).

Animals were sacrificed 3 weeks after the OVX (i.e., Day 101). Our past experience and others showed up to a 20% loss in bone mass 3 weeks following OVX in rats (31). Skin from the dorsal surface, liver and both femurs were collected.

Tissue specimens were analyzed blindly for total Gd^{3+} concentration by inductively coupled plasma mass spectrometry (ICP-MS) at Guerbet Research laboratories, France. Histological examination, electron microscopic (EM) and energy filtered transmission electron microscopy (EFTEM) evaluations of skin specimens at the Central EM-Lab, Medical Center Regensburg, Germany, were blinded.

Inductively-coupled plasma mass spectrometry (ICP-MS)

Serum (100 µL), bone (500 mg), skin (400 mg) and liver (1-2 g) samples were mineralized in 65% HNO_3 (overnight, 80 ℃). The total concentration of Gd^{3+} in the tissues was measured by ICP-MS (ELAN DRC Plus® mass spectrometer, Perkin Elmer Life and Analytical Sciences Inc., Waltham, MA, USA). A standard curve of inorganic Gd^{3+} (0.64 nmol/L-7.63 µmol/L) in 6.5% HNO_3 was employed by monitoring the response of the ^{157}Gd isotope. Variation of signal was corrected by the addition of indium. The limit of assay quantification was 0.64 nmol/L.

Light microscopic examination

Skin specimens were fixed in neutral buffered formalin overnight. The 4-µm-thick sections were obtained from formalin-fixed and paraffin-embedded specimens. Then the sections were stained with haematoxylin and eosin. The nuclei number of spindle cells and stellate cells was counted with tissue areas containing hair follicles, sweat glands, blood vessels or fat cells avoided. The cell number in five random vision fields of each slide was counted. Cellularity was defined by the number of spindle cells and stellate cells under the epidermis layer per ×200 vision field. The average epidermis thickness was measured in ten random vision fields (×200). All quantitative procedures were carried out by a blinded reader.

Electron microscopy

Skin samples included those of phase 1 study (n=8 rats, from control, gadodiamide and gadoterate meglumine groups), and of phase 2 study (n=8 rats, from control + OVX, gadodiamide, and gadodiamide + OVX groups). They were primarily fixed in buffered formalin, and then subdivided in smaller pieces (approx. 2 mm^3) and additionally fixed in 4% glutaraldehyde. All samples were post-fixed in 1% osmium tetroxide, routinely processed with automated tissue processor LYNX/Leica, and embedded in epon resin blocks.

Semi-thin sections (0.8 µm, double staining toluidine blue/basic fuchsine) were prepared and evaluated by light microscopy for orientation and tissue area trimming for electron microscopic study. Selected blocks were ultrathin sectioned (80 nm, contrasted with uranyl and lead salt solutions) and examined with transmission electron microscopy (Zeiss LEO912AB Energy Filtering Transmission Electron Microscopy). Elemental analysis was performed with electron energy loss spectroscopy (EELS) and electron spectroscopic imaging (ESI).

Energy filtered transmission electron microscopy (EFTEM)

EFTEM microanalysis for gadolinium and iron deposits

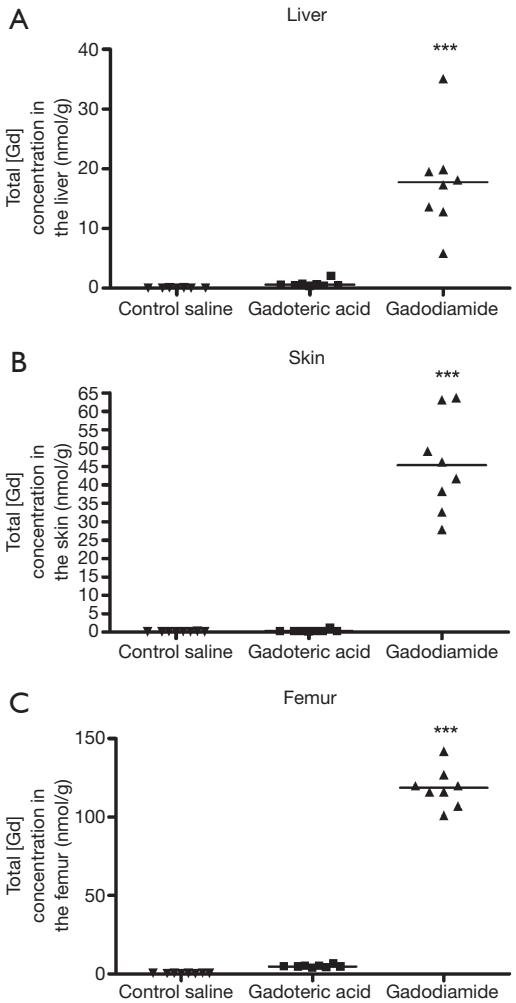

Figure 1 Phase one study. Total gadolinium concentration (nmol/g, by ICP-MS measurement) observed in liver (A), skin (B) and bone (C) samples of rats receiving saline (control), gadodiamide or gadoteric acid. Significant higher concentration was noted in the liver, skin, and bone (femur) of the rats following gadodiamide administration than following gadoteric acid administration. ***, P<0.001 *vs.* other groups. Gd, gadolinium.

was performed on 40 nm unstained sections. Parallel EELS in the spot mode (Zeiss LEO912AB/Oberkochen; iTEM software package OSIS/Muenster, Germany) was used to analyse the intracellular and collagen fibril associated electron dense areas suspected of containing Gd^{3+} and/or $Fe^{2+/3+}$. Gd^{3+} produced characteristic white line M4,5 edge at 1,185 eV, the iron ionisation L2,3 edge is at 708 eV in the EELS spectrum. The spatial distribution of the elements was mapped by ESI applying the three window method, using inelastically scattered electrons with the element-specific energy loss.

Statistical analysis

Data are expressed as mean ± standard deviation. Difference in cellularity and epidermis thickness among animal groups, and Gd concentration were tested with one-way ANOVA. In the case of a significant difference, pairwise comparisons were performed using a Bonferroni's test. A P value <0.05 was considered statistically significant.

Results

Phase 1 study

Gd tissue concentration measurement

Gd^{3+} concentration was 180-fold higher in the skin in rats receiving gadodiamide than rats treated with gadoteric acid, 25-fold higher in the femur and 30-fold higher in the liver (P<0.001) (*Figure 1*). The highest total Gd^{3+} concentration was found in femur samples (*Figure 1*). No difference was observed in left and right femurs. No significant difference was observed between gadoteric acid group and the control rats regardless the tissue.

Light microscopy findings

The collagen fibril under epidermis layer displayed different density among the three groups. Gadodiamide treated rats exhibited highest collagen fibril density, and control rats demonstrated normal collagen fibril density (*Figure 2*). There were more spindle and stellate cells under epidermis layer in gadodiamide rats compared with gadoteric acid exposure rats. Meanwhile, the gadoteric acid-treated rats also showed more spindle cells and stellate cells than the control group (*Figure 2*, *Table 1*). The gadodiamide-treated rats showed the thickest epidermis layer, whereas the saline-treated group exhibited normal epidermis layer (*Figure 3*). No histological difference was observed between the baseline and saline-treated rat skins at week 10.

Electron microscopy and elemental analysis

The EM examination of all skin sections showed normal ultrastructural architecture of the epidermis and dermis with some additional findings in the gadodiamide group only. One of the biopsy displayed extended diameters of the collagen but without profile deformations (*Figure 4A*). In another skin specimen a multifocal "halo" formation

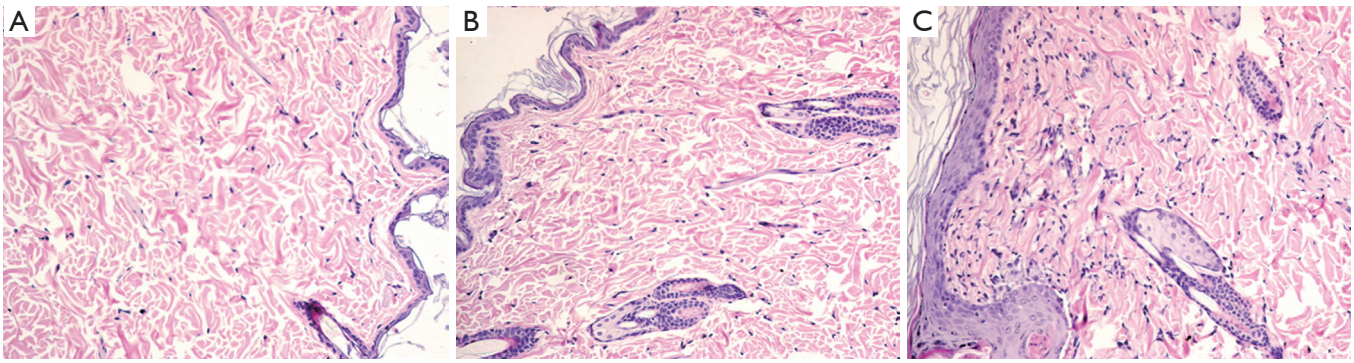

Figure 2 Phase 1 study. HE histology (original magnification, ×200). (A) Saline-treated rats showed normal collagen fibril density; (B) gadoteric acid and (C) gadodiamide induced spindle cell and stellate cell hyperplasia, and resulted in denser collagen fibril. The gadodiamide-treated rats show thicker epidermis layer and more abundant and denser collagen fibril than the gadoteric acid treated rats.

Table 1 Cellularity and epidermal thickness of rats treated with saline, gadoteric acid, and gadodiamide in phase 1 study

Study group	Cellularity/×200 view*	Epidermis thickness (μm)**
Baseline	89±10	22±4
Saline	90±7	25±5
Gadoteric acid	104±10$^{\#}$	33±4$^{\Delta}$
Gadodiamide	120±9§	46±9$^{\Delta}$

*, 8 rats × 5 fields = 40 counts; **, 8 rats × 10 fields = 80 counts. Cellularity was defined by the number of spindle cells and stellate cells under the epidermis layer per vision field (×200). Cellularity: $^{\#}$, P=0.002 *vs.* saline group; §, P<0.0001 *vs.* saline group; gadodiamide group *vs.* gadoteric acid group P=0.001. Epidermis thickness (Δ), saline *vs.* gadoteric acid; gadoteric acid *vs.* gadodiamide, both <0.001.

consisting of fuzzy material around or close to singular collagen fibre was noticed in some collagen bundles (*Figure 4B*). The "halo" area had a mean diameter of 732 nm. Additionally Gd^{3+}-positive deposits were associated with some of the fibres involved in the "halo" formation (*Figure 4C*). Six of the eight screened skin specimens (75%) showed randomly dispersed singular collagen fibre with Gd deposition or incrustation in the dermis, as confirmed by EELS-analysis (*Figure 4A*,*D*,*E*). These depositions displayed a fine needle and/or filamentous texture (measured needle/filament thickness was approximately 2 nm). In five skin specimens, intracellular membrane-bound Gd^{3+}-positive inclusions with granular texture were found sporadically in some fibroblasts and smooth muscle cells in perifollicular localization (*Figure 4F*). Positive $Fe^{2+/3+}$-signal was recorded in membrane-bound inclusions of some fat droplet associated cells in two skin specimens from the deep dermis of eight examined.

Phase 2 study

Gadolinium tissue concentration measurement

No significant differences in total Gd^{3+} concentration in liver, skin, and femur were observed between rats received gadodiamide and with OVX or not (*Figure 5*).

Light microscopy findings

There was no difference in skin thickness and skin cellularity between the gadodiamide rats and gadodiamide + OVX rats (*Figures 6*,*7*). For both cellularity and epidermis thickness, there was no significant difference between baseline value and saline + OVX group, but there was significant difference between the gadodiamide treated rats (with or without OVX) and saline treated rats (P<0.01) (*Table 2*).

Electron microscopy and elemental analysis

Skin sections from the gadodiamide and gadodiamide + OVX rats revealed similar findings as in phase one study. Calibre variation of the collagen fibres was noted in both groups without fibre profile abnormality. Gd^{3+}-deposits associated with singular collagen fibrils were found multi-spotted in collagen bundles in both groups (*Figure 8A*). "Halo" formation around collagen fibrils was observed. Additionally, Gd^{3+}-deposits were found associated with elastic fibres in the skin of the gadodiamide treated rats (*Figure 8B*). Cytoplasmic membrane-bound (lysosomal)

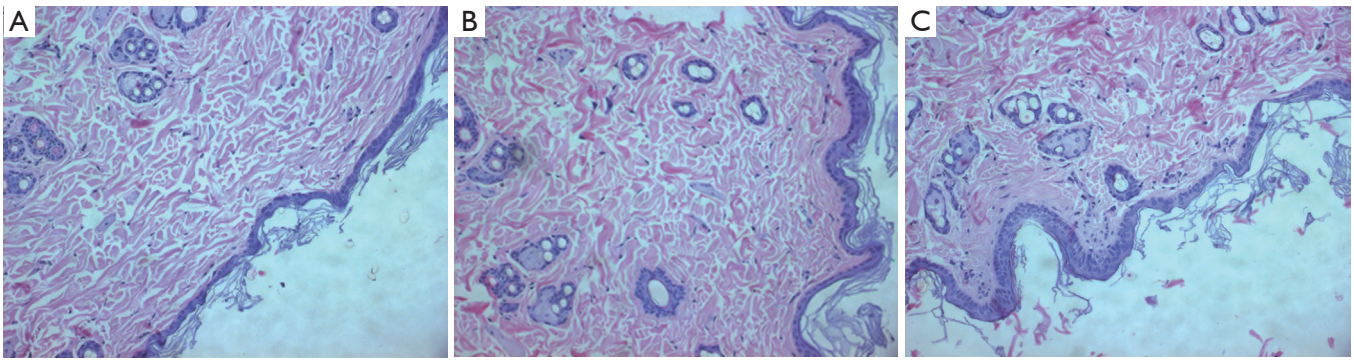

Figure 3 Phase 1 study. HE histology (original magnification, ×200) shows thickness of epidermis layer in saline treated rat (A), gadoterate meglumine treated rat (B), gadodiamide treated rat (C). Gadodiamide treated rats have the thickest epidermis layer, followed by the gadoterate meglumine treated rats. Saline treated rats show normal epidermis layer thickness.

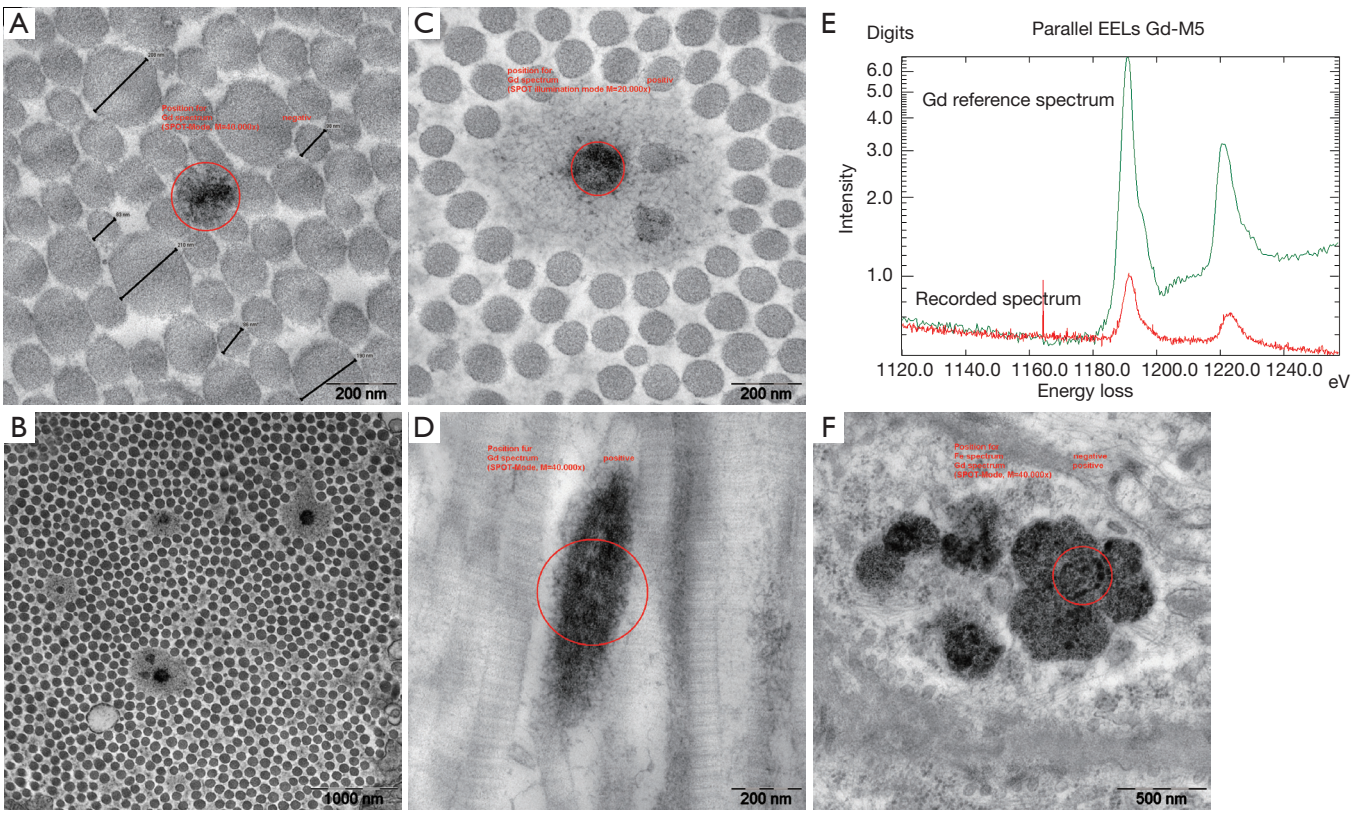

Figure 4 Phase 1 study. EM reveals alterations of collagen fibres and lysosomal Gd deposition in the gadodiamide treated rats. (A) Collagen fibre diameter variation in a collagen bundle without abnormalities in the fibre profile. Note one fibre with Gd^{3+} incrustations (circle represents the area analysed by the EELS elemental analysis); (B) example of a collagen bundle with typical distribution of some collagen fibres surrounded by "halo" formation, overview; (C) detail showing the extend of the "halo" phenomenon including three collagen fibres and one with a dark Gd^{3+} deposition; (D) longitudinal section of a collagen fibre with dark Gd incrustation displaying a fuzzy filamentous texture; (E) corresponding recorded EELS spectrum from the area encircled in image D confirming Gd^{3+} content in the analyzed deposition (red = recorded sample spectrum; green = Gd reference spectrum); (F) example of multiple lysosomal Gd^{3+} rich inclusions with granular texture in perifollicular smooth muscle cells. Gd, gadolinium; EELS, electron energy loss spectroscopy.

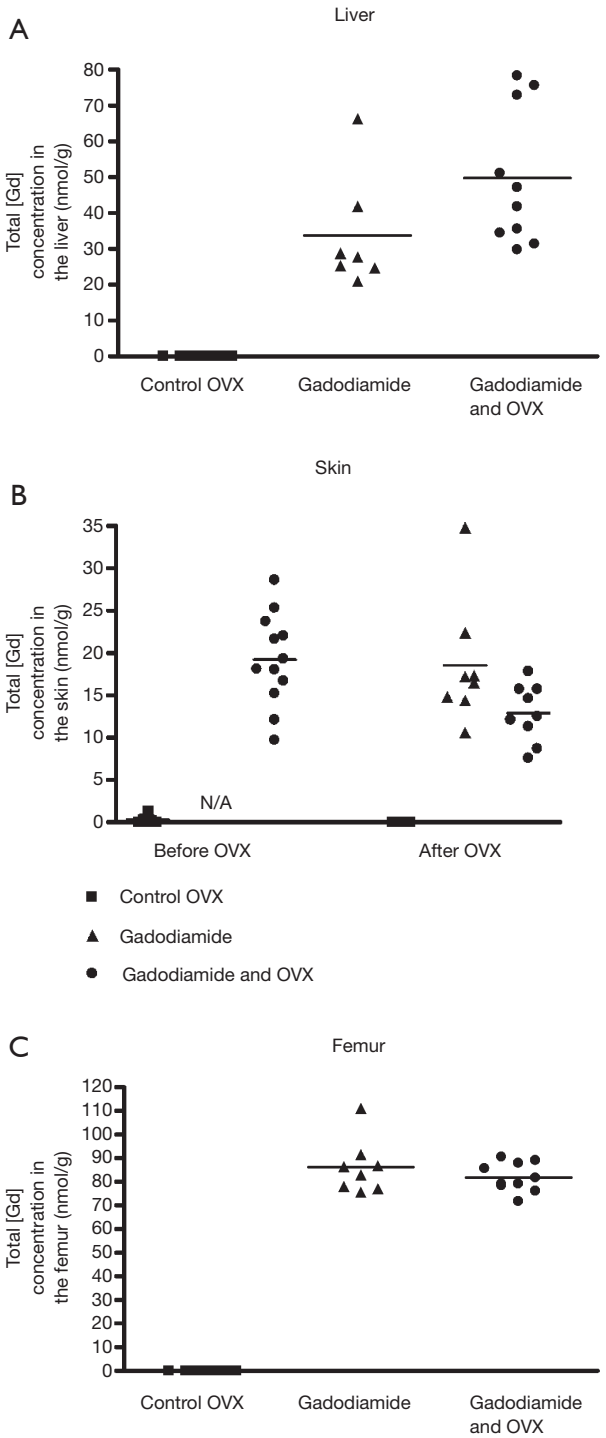

Figure 5 Phase 2 study. Total Gd^{3+} concentration (nmol/g, ICP-MS measurement) in liver (A), skin (B); and bone (C) samples of rats receiving gadodiamide with or without OVX and of control rats. OVX, ovariectomy; Gd, gadolinium.

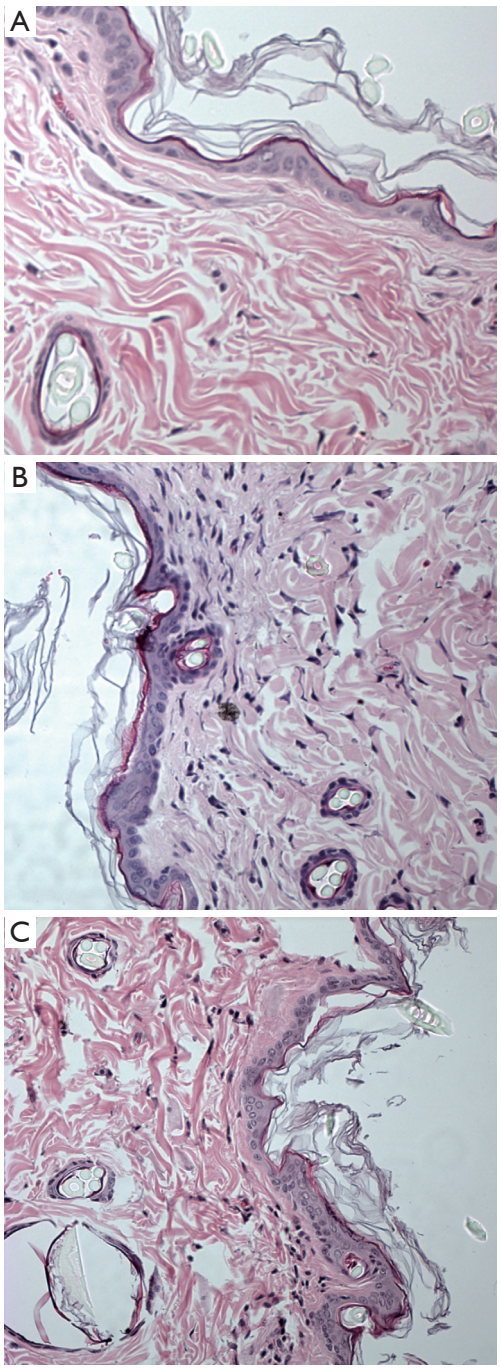

Figure 6 Phase 2 study. HE histology (original magnification, × 200) shows normal collagen fibril density under the epidermis layer in (A), obtained from saline-treated rats underwent OVX. Both in gadodiamide only (B) and in gadodiamide + OVX -treated rats (C), -treated rats, spindle cell and stellate cell hyperplasia were found, resulting in denser collagen fibril. OVX, ovariectomy.

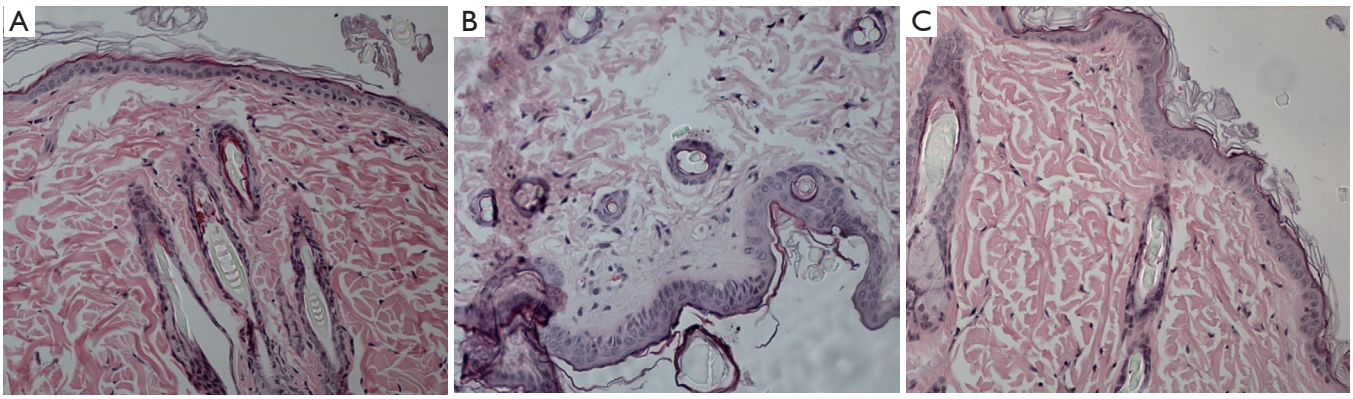

Figure 7 Phase 2 study. HE histology (original magnification, ×200) shows the thickness of epidermis layer in a saline treated rat underwent OVX (A), a gadodiamide treated only rat (B), and a gadodiamide + OVX treated rat (C). Saline treated rat underwent OVX show normal epidermis layer thickness, while gadodiamide treated only rat and gadodiamide + OVX treated rat have similarly thickened epidermis layer. OVX, ovariectomy.

Table 2 Cellularity and epidermis thickness of rats treated with saline + OVX, gadodiamide only, and gadodiamide + OVX in phase 2 study

Study group	Cellularity/× 200 view*	Epidermis thickness (μm)**
Baseline	94±7	24±2
Saline + OVX	101±4	26±2
Gadodiamide	126±8 §	41±3 §
Gadodiamide + OVX	124±6 §	39±5 §

*, 8 rats × 5 fields =40 counts; **, 8 rats × 10 fields =80 counts. Cellularity was defined by the number of spindle cells and stellate cells under the epidermis layer per vision field (×200). §, P<0.001 *vs.* saline group; P>0.05 gadodiamide group *vs.* gadodiamide + OVX group. OVX, ovariectomy.

gadolinium deposits with granular texture were identified in some fibrocytes of both groups (*Figure 8C*). Lysosomal iron-positive inclusions were occasionally observed in some fat tissue associated cells. Co-localization of Gd^{3+} and $Fe^{2+/3+}$ in the same lysosome or cell was observed in both groups (*Figure 8D-F*). No inclusion was observed in the perifollicular smooth muscle cells.

Discussion

In several animal studies, highest total Gd^{3+} retention in tissues have been reported with non-ionic linear GBCAs while minimal retention was observed with the more thermodynamically stable macrocyclic agents (10-16,32). Similar findings were observed in the present study with repeated injections of high dosage of GBCAs, with the non-ionic linear gadodiamide producing much higher tissue retention of Gd^{3+} than the ionic macrocyclic chelate gadoteric acid. Interestingly, compared with liver and skin, Gd^{3+} concentration was much higher in femur following gadodiamide administration. It has been suggested that Gd^{3+} deposition in bone was due to free Gd^{3+} released from the GBCA by transmetallation (and subsequently incorporated into the carbonated calcium hydroxyapatite of bone tissue (17). Gd^{3+} and other lanthanides are thought to substitute calcium in hydroxyapatite lattice of the bone matrix (33). However, the actual accumulation mechanisms of the lanthanides in bone remain poorly understood (34).

During bone resorption, osteoclasts secret proteinases and hydrochloric acid to dissolve existing bone mineral by creating an acidic condition of an approximate pH of 4.5 (35), which may theoretically facilitate the release of Gd^{3+} from the hydroxyapatite complex into the circulation, leading to deposition of the released Gd^{3+} into other tissues. Significantly lower Gd^{3+} concentrations, in both cortical and trabecular tissues, have been observed in fracture osteoporotic patients than in osteoarthritis patients (25).

To our knowledge, this is the first study investigating the Gd^{3+} uptake in bone tissue in an experimental model associated with high bone turnover. Three weeks after bilateral OVX, bone loss is approximately 15-20% (29-31). This extent of bone resorption was comparable to that

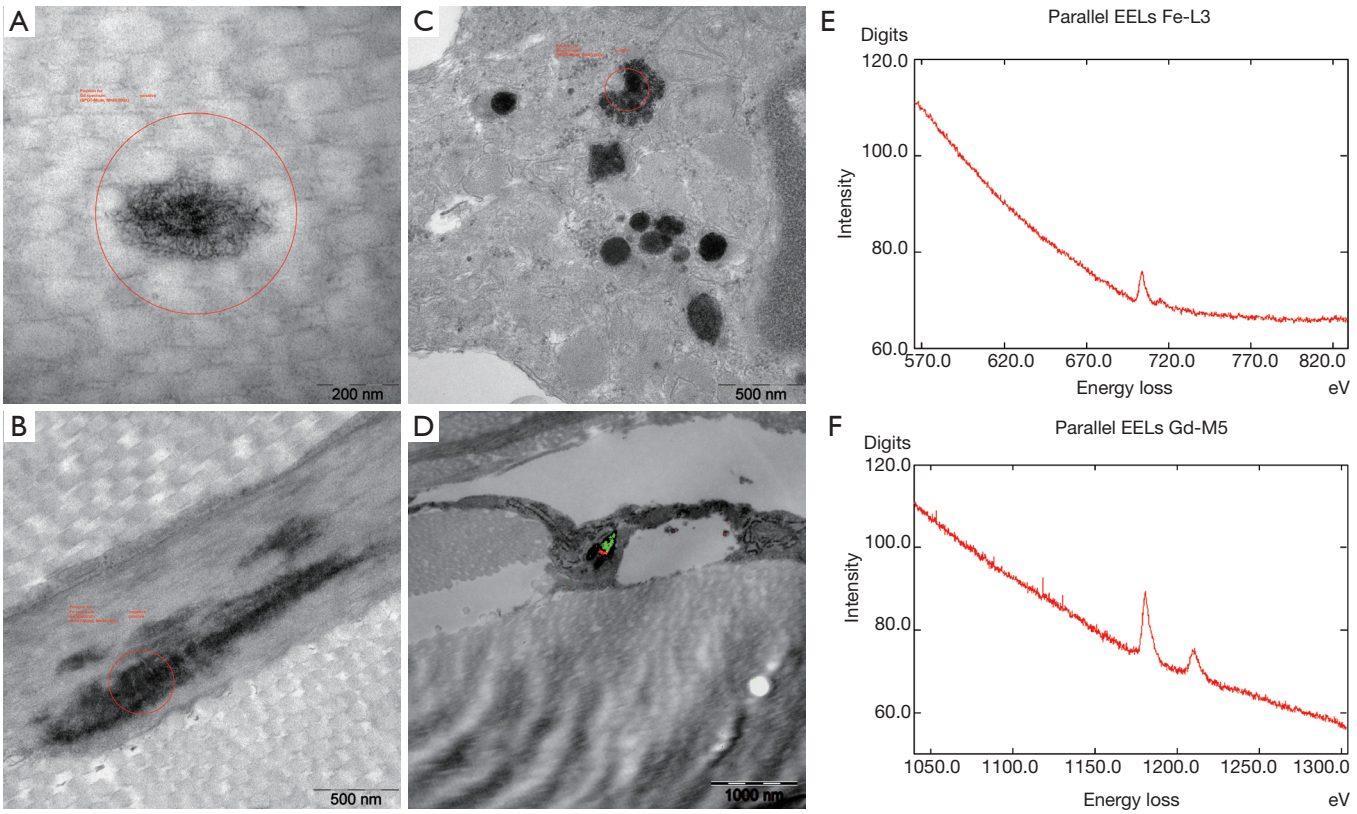

Figure 8 Phase 2 study. EM findings in gadodiamide treated rat and gadodiamide + OVX rat. EM shows Gd^{3+} deposits associated mainly with dermal collagen and elastic fibres, and some fibroblasts. (A) High power magnification displays the filamentous texture of the collagen fibre Gd^{3+} incrustation in a gadodiamide + ovariectomy treated rat; (B) example of an elastic fibre with dark Gd^{3+}-rich deposition in a gadodiamide only treated animal; (C) multiple dark lysosomal granular Gd^{3+} deposits in fibroblasts of a gadodiamide + ovariectomised rat; (D) elemental mapping by the ESI method (red = Gd^{3+}, green = $Fe^{2+/3+}$) revealed the spatial $Fe^{2+/3+}$ and Gd^{3+} colocalization in the lysosome of fat associated cells; (E,F) documentation of corresponding recorded positive Fe and Gd EELS spectra of the lysosomal inclusion mapped in image D. Gd, gadolinium; EELS, electron energy loss spectroscopy.

observed in post-menopausal women which range between 19-26%. The cumulated dose administered to rats in this study was in the same range as that selected in other rat studies (11-16). In this study we did not observe reduction of the extent of Gd^{3+} retention in bone or increase in the Gd^{3+} content of skin and liver with the development of osteoporosis. However, as this study was carried out in a single time-point, i.e., OVX performed 60 days after gadodiamide injection and animals were sacrificed 3 weeks later, a further time-course study may be of interest and may provide further insights.

The Gd^{3+} deposition in skin of animals with marked reduction in renal function was detected extracellularly within collagen bundles, and intracellularly within the fibroblast associated with collagen fibril fragments. Interestingly, this effect has been observed with gadodiamide but not with the macrocyclic agent gadoteric acid (16). The process of the Gd^{3+} deposition is presumptive and most likely due to dissociation of low thermodynamic stability GBCAs in the extracellular extravascular compartment of the skin (17). Luminescence studies also demonstrated direct binding of lanthanides to collagen with five or less lanthanide ion binding sites per molecule. Lanthanides are also known to enhance the polymerisation of skin collagen (36,37).

The ultrastructural changes in the dermis after administration of GBCAs in animals with normal renal function have not been studied before. In this study we demonstrated gadolinium deposits in the skins of rats with and without OVX treated with gadodiamide. Gd^{3+}-deposits

collagen bundles were observed preferentially in the deep dermis. Cytoplasmic membrane-bound (lysosomal) Gd^{3+}-deposits with granular texture were identified in some fibrocytes, smooth muscle, and fat tissue associated cells. Lysosomal iron-positive inclusions were occasionally observed in fibroblasts and some fat tissue associated cells, co-localisation of Gd^{3+} and $Fe^{2+/3+}$ in the same lysosome or cell was noted in rats with and without OVX treated with gadodiamide. In the skin of one gadodiamide-treated rat, a "halo" formation around a number of collagen fibrils was noted. This phenomenon has already been observed in a previous study in rats with reduced renal function (16) as well as in the skin of an NSF patient (23). While the nature of the halo is unclear, it is possible that the Gd^{3+} incrustation of the collagen protofilaments prevents the normal fibre polymerization and cause the "halo" phenomenon around the affected fibres.

The ultrastructural changes observed in OVX rats were comparable to normal rats after exposure to gadodiamide. The increase in dermal cellularity after exposure to gadodiamide was observed in previous animal studies and in NSF patients (5,17,38). The observed increase in epidermal thickness may represent another feature of skin reaction to Gd^{3+} deposition. Some increase in the dermal cellularity and epidermal thickness was also observed with gadoteric acid but to a much lesser extent in comparison to rats treated with gadodiamide. Previous rat studies showed no histological changes in the skin after exposure to gadoteric acid (13-16) and this observation in our study cannot be fully explained, but probably related to high dosage used in this study.

Conclusions

Total Gd^{3+} tissue retention with gadodiamide was significantly higher than with gadoteric acid in healthy rats. Ultrastructural changes in the skin after gadodiamide exposure included focal Gd^{3+} deposition/incrustation of collagen fibres with a "halo" formation around some fibres. These changes were absent with the macrocyclic gadoteric acid. Osteoporosis did not alter total Gd^{3+} deposition in tissues following administration of gadodiamide to ovariectomised rats in this study.

Acknowledgements

We are grateful for Dr Feng Zhao and Dr Tao Gu for help in parts of the animal experiments.

Footnote

Conflicts of Interest: JM Idée, N Fretellier, G Jestin-Mayer, and C Factor are employee of Guerbet Group, France. Guerbet markets contrast agents and specifically gadoteric acid (Dotarem®) mentioned in this study. Other authors declare no conflicts of interest.

References

1. Sieber MA, Pietsch H, Walter J, Haider W, Frenzel T, Weinmann HJ. fibrosis: a possible role for gadolinium-based contrast media. Invest Radiol 2008;43:65-75.
2. Sieber MA, Lengsfeld P, Frenzel T, Golfier S, Schmitt-Willich H, Siegmund F, Walter J, Weinmann HJ, Pietsch H. Preclinical investigation to compare different gadolinium-based contrast agents regarding their propensity to release gadolinium in vivo and to trigger nephrogenic systemic fibrosis-like lesions. Eur Radiol 2008;18:2164-73.
3. Idée JM, Port M, Robic C, Medina C, Sabatou M, Corot C. Role of thermodynamic and kinetic parameters in gadolinium chelate stability. J Magn Reson Imaging 2009;30:1249-58.
4. Morcos SK. Nephrogenic systemic fibrosis following the administration of extracellular gadolinium based contrast agents: is the stability of the contrast agent molecule an important factor in the pathogenesis of this condition? Br J Radiol 2007;80:73-6.
5. Morcos SK, Thomsen HS. Nephrogenic systemic fibrosis: more questions and some answers. Nephron Clin Pract 2008;110:c24-31; discussion c32.
6. Liu H, Yuan L, Yang X, Wang K. La(3+), Gd(3+) and Yb(3+) induced changes in mitochondrial structure, membrane permeability, cytochrome c release and intracellular ROS level. Chem Biol Interact 2003;146:27-37.
7. Pałasz A, Czekaj P. Toxicological and cytophysiological aspects of lanthanides action. Acta Biochim Pol 2000;47:1107-14.
8. Tweedle MF, Wedeking P, Kumar K. Biodistribution of radiolabeled, formulated gadopentetate, gadoteridol, gadoterate, and gadodiamide in mice and rats. Invest Radiol 1995;30:372-80.
9. Bousquet JC, Saini S, Stark DD, Hahn PF, Nigam M, Wittenberg J, Ferrucci JT Jr. Gd-DOTA: characterization

of a new paramagnetic complex. Radiology 1988;166:693-8.
10. Wadas TJ, Sherman CD, Miner JH, Duncan JR, Anderson CJ. The biodistribution of [153Gd]Gd-labeled magnetic resonance contrast agents in a transgenic mouse model of renal failure differs greatly from control mice. Magn Reson Med 2010;64:1274-80.
11. Pietsch H, Lengsfeld P, Jost G, Frenzel T, Hütter J, Sieber MA. Long-term retention of gadolinium in the skin of rodents following the administration of gadolinium-based contrast agents. Eur Radiol 2009;19:1417-24.
12. Fretellier N, Idée JM, Dencausse A, Karroum O, Guerret S, Poveda N, Jestin G, Factor C, Raynal I, Zamia P, Port M, Corot C. Comparative in vivo dissociation of gadolinium chelates in renally impaired rats: a relaxometry study. Invest Radiol 2011;46:292-300.
13. Fretellier N, Idée JM, Guerret S, Hollenbeck C, Hartmann D, González W, Robic C, Port M, Corot C. Clinical, biological, and skin histopathologic effects of ionic macrocyclic and nonionic linear gadolinium chelates in a rat model of nephrogenic systemic fibrosis. Invest Radiol 2011;46:85-93.
14. Fretellier N, Idée J, Bruneval P, Guerret S, Daubiné F, Jestin G, Factor C, Poveda N, Dencausse A, Massicot F, Laprévote O, Mandet C, Bouzian N, Port M, Corot C. Hyperphosphataemia sensitizes renally impaired rats to the profibrotic effects of gadodiamide. Br J Pharmacol 2012;165:1151-62.
15. Fretellier N, Bouzian N, Parmentier N, Bruneval P, Jestin G, Factor C, Mandet C, Daubiné F, Massicot F, Laprévote O, Hollenbeck C, Port M, Idée JM, Corot C. Nephrogenic systemic fibrosis-like effects of magnetic resonance imaging contrast agents in rats with adenine-induced renal failure. Toxicol Sci 2013;131:259-70.
16. Haylor J, Schroeder J, Wagner B, Nutter F, Jestin G, Idée JM, Morcos S. Skin gadolinium following use of MR contrast agents in a rat model of nephrogenic systemic fibrosis. Radiology 2012;263:107-16.
17. Idée JM, Fretellier N, Robic C, Corot C. The role of gadolinium chelates in the mechanism of nephrogenic systemic fibrosis: A critical update. Crit Rev Toxicol 2014;44:895-913.
18. High WA, Ayers RA, Chandler J, et al. Gadolinium is detectable within the tissue of patients with nephrogenic systemic fibrosis. J Am Acad Dermatol 2007;56:21-6.
19. Boyd AS, Zic JA, Abraham JL. Gadolinium deposition in nephrogenic fibrosing dermopathy. J Am Acad Dermatol 2007;56:27-30.
20. Abraham JL, Chandra S, Thakral C, Abraham JM. SIMS imaging of gadolinium isotopes in tissue from Nephrogenic Systemic Fibrosis patients: Release of free Gd from magnetic resonance imaging (MRI) contrast agents. Appl Surf Sci 2008;255:1181-4.
21. Abraham JL, Thakral C. Tissue distribution and kinetics of gadolinium and nephrogenic systemic fibrosis. Eur J Radiol 2008;66:200-7.
22. Abraham JL, Thakral C, Skov L, Rossen K, Marckmann P. Dermal inorganic gadolinium concentrations: evidence for in vivo transmetallation and long-term persistence in nephrogenic systemic fibrosis. Br J Dermatol 2008;158:273-80.
23. Schroeder JA, Weingart C, Coras B, Hausser I, Reinhold S, Mack M, Seybold V, Vogt T, Banas B, Hofstaedter F, Krämer BK. Ultrastructural evidence of dermal gadolinium deposits in a patient with nephrogenic systemic fibrosis and end-stage renal disease. Clin J Am Soc Nephrol 2008;3:968-75.
24. White GW, Gibby WA, Tweedle MF. Comparison of Gd(DTPA-BMA) (Omniscan) versus Gd(HP-DO3A) (ProHance) relative to gadolinium retention in human bone tissue by inductively coupled plasma mass spectroscopy. Invest Radiol 2006;41:272-8.
25. Darrah TH, Prutsman-Pfeiffer JJ, Poreda RJ, Ellen Campbell M, Hauschka PV, Hannigan RE. Incorporation of excess gadolinium into human bone from medical contrast agents. Metallomics 2009;1:479-88.
26. Yuan G, Lu H, Yin Z, Dai S, Jia R, Xu J, Song X, Li L. Effects of mixed subchronic lead acetate and cadmium chloride on bone metabolism in rats. Int J Clin Exp Med 2014;7:1378-85.
27. Spencer AJ, Wilson SA, Batchelor J, Reid A, Rees J, Harpur E. Gadolinium chloride toxicity in the rat. Toxicol Pathol 1997;25:245-55.
28. Morcos SK. Sheffield 2nd International Workshop on experimental studies of nephrogenic systemic fibrosis, 15th June 2012, Sheffield, UK. Quant Imaging Med Surg 2012;2:147-50.
29. Deng M, Wang YX, Griffith JF, Lu G, Ahuja AT, Poon WS. Characteristics of rat lumbar vertebral body bone mineral density and differential segmental responses to sex hormone deficiency: a clinical multidetector computed tomography study. Biomed Environ Sci 2012;25:607-13.
30. Wang YX, Griffith JF, Zhou H, Choi KC, Hung VW, Yeung DK, Qin L, Ahuja AT. Rat lumbar vertebrae bone densitometry using multidetector CT. Eur Radiol 2009;19:882-90.

31. Griffith JF, Wang YX, Zhou H, Kwong WH, Wong WT, Sun YL, Huang Y, Yeung DK, Qin L, Ahuja AT. Reduced bone perfusion in osteoporosis: likely causes in an ovariectomy rat model. Radiology 2010;254:739-46.
32. Haylor J, Dencausse A, Vickers M, Nutter F, Jestin G, Slater D, Idee JM, Morcos S. Nephrogenic gadolinium biodistribution and skin cellularity following a single injection of Omniscan in the rat. Invest Radiol 2010;45:507-12.
33. Vidaud C, Bourgeois D, Meyer D. Bone as target organ for metals: the case of f-elements. Chem Res Toxicol 2012;25:1161-75.
34. Morcos SK. Experimental studies investigating the pathophysiology of nephrogenic systemic fibrosis; what did we learn so far? Eur Radiol 2011;21:496-500.
35. Teitelbaum SL. Bone resorption by osteoclasts. Science 2000;289:1504-8.
36. Drouven BJ, Evans CH. Collagen fibrillogenesis in the presence of lanthanides. J Biol Chem 1986;261:11792-7.
37. Evans CH, Drouven BJ. The promotion of collagen polymerization by lanthanide and calcium ions. Biochem J 1983;213:751-8.
38. Girardi M, Kay J, Elston DM, Leboit PE, Abu-Alfa A, Cowper SE. Nephrogenic systemic fibrosis: clinicopathological definition and workup recommendations. J Am Acad Dermatol 2011;65:1095-106.e7.

Cite this article as: Wáng YX, Schroeder J, Siegmund H, Idée JM, Fretellier N, Jestin-Mayer G, Factor C, Deng M, Kang W, Morcos SK. Total gadolinium tissue deposition and skin structural findings following the administration of structurally different gadolinium chelates in healthy and ovariectomized female rats. Quant Imaging Med Surg 2015;5(4):534-545. doi: 10.3978/j.issn.2223-4292.2015.05.03

